



Optimal array layout of cylindrical baffles to reduce energy of rock avalanche

Yu-zhang BI, Dong-po WANG, Xian-lei FU, Yi-xiong LIN, Xin-po SUN, Zhe-yuan JIANG

View online: <https://doi.org/10.1007/s11629-021-6916-y>

Articles you may be interested in

Centrifuge and numerical modeling of h-type anti-slide pile reinforced soil-rock mixture slope

Journal of Mountain Science. 2023, 20(5): 1441 <https://doi.org/10.1007/s11629-022-7446-y>

Numerical investigation of rock dynamic fragmentation during rockslides using a coupled 3D FEM-DEM method

Journal of Mountain Science. 2022, 19(4): 1051 <https://doi.org/10.1007/s11629-021-6930-0>

Identification of hidden faults using determining velocity structure profile by spatial autocorrelation method in the west of Mashhad plain (Northeast of Iran)

Journal of Mountain Science. 2021, 18(12): 3261 <https://doi.org/10.1007/s11629-020-6511-7>

Characteristics and dynamics of the Ganqiuchi rock avalanche triggered by a paleo-earthquake in the Northern Qinling Mountains


Journal of Mountain Science. 2020, 17(5): 1143 <https://doi.org/10.1007/s11629-019-5599-0>


Landslide dynamic process and parameter sensitivity analysis by discrete element method: the case of Turnoff Creek rock avalanche


Journal of Mountain Science. 2020, 17(7): 1581 <https://doi.org/10.1007/s11629-020-5993-7>


Original Article


Optimal array layout of cylindrical baffles to reduce energy of rock avalanche


BI Yu-zhang¹  <https://orcid.org/0000-0003-2631-6620>; e-mail: yuzhang.bi@bzgeotech.com

WANG Dong-po^{2*}  <https://orcid.org/0000-0002-6172-4753>; e-mail: wangdongpo2014@cdut.edu.cn

FU Xian-lei¹  <https://orcid.org/0000-0002-9668-7921>; e-mail: fuxianlei@bzgeotech.com

LIN Yi-xiong^{1*}  <https://orcid.org/0000-0001-6331-9594>; e-mail: yixionglin@outlook.com

SUN Xin-po³  <https://orcid.org/0000-0001-8973-9853>; e-mail: xinpohd@163.com

JIANG Zhe-yuan^{1,4}  <https://orcid.org/0000-0002-8207-3478>; e-mail: research@bzgeotech.com

*Corresponding author

¹ B-Z geotechnical Company, Nanjing 210096, China

² State Key Laboratory of Geohazard Prevention and Geoenvironment Protection, Chengdu University of Technology, Chengdu 610059, China

³ College of Civil Engineering, Sichuan University of Science and Engineering, Zigong 643000, China

⁴ Jiangsu Key Laboratory of Urban Underground Engineering & Environmental Safety, Institute of Geotechnical Engineering, Southeast University, Nanjing 210096, China

Citation: Bi YZ, Wang DP, Fu XL, et al. (2022) Optimal array layout of cylindrical baffles to reduce energy of rock avalanche. Journal of Mountain Science 19(2). <https://doi.org/10.1007/s11629-021-6916-y>

© Science Press, Institute of Mountain Hazards and Environment, CAS and Springer-Verlag GmbH Germany, part of Springer Nature 2022

Abstract: The array of baffles protection structure is a flow resistance structure with good drainage, blocking, and intercepting effects on the rock avalanches. In this research, the physical model test on rock avalanches was conducted. Three parameters (column spacing, row spacing, and a number of baffles) were used as indicators to determine the optimal layout of the array of baffles for energy efficiency consumption blocking. Then, the lattice Boltzmann numerical simulation method was used to build a numerical simulation model of rock avalanches-array of the baffles-hazard-bearing body to obtain the rock's velocity attenuation and flow trajectory avalanches in the impact baffle protection structure. Finally, the results of the physical model test and the numerical simulation were mutually

confirmed. The following conclusions were drawn through two methods of physical model test and numerical simulation. (1) The optimal layout parameters of array of baffles were determined as three rows of array of baffles (The number of baffles in each row is 7, 8, 9), column spacing $Sc=3.5$, and row spacing $Sr=4.5$. (2) Under the conditions of high baffle density (such as $Sc=1.5, 2.5$), the rock avalanches would produce a certain degree of circumfluence, which would increase the fluid velocity by at least 24.5% over the average velocity, so the column spacing density should be increased appropriately to achieve the optimal effect of reducing the energy of rock avalanches. (3) In the event of a prototype grooved rock avalanches with a velocity close to 24.5 m/s and a flow depth of about 1.5 m, the three-row array of baffles protection with the parameters $Sc^*=1.18$ m and $Sr^*=1.51$ m could be arranged, playing the role of optimizing the array of

Received: 27-May-2021

1st Revision: 17-Jul-2021

2nd Revision: 26-Aug-2021

Accepted: 31-Aug-2021

baffles to guide the flow and block the energy consumption. LBM experiments can be used to replace laboratory experiments to some extent. Further Lattice Boltzmann method-Discrete element method (LBM-DEM) studies are required before applications to practical engineering.

Keywords: Lattice Boltzmann; Physical model; Numerical simulation; Energy consumption optimization

Notation:

Abbreviation	Explanation
$(Fr)_m$	Model Froude number
$(Fr)_p$	Prototype Froude number
γ_v	Fluid velocity similarity ratio
v_p	Prototype fluid velocity
v_m	Model fluid velocity
γ_h	Fluid depth similarity ratio
h_p	Prototype fluid depth
h_m	Model fluid depth
α	Slope angle
$LS1$	Slope length 1
$LS2$	Slope length 2
m_1	Length of Row 1
m_2	Length of Row 2
m_3	Length of Row 3
r	Baffle diameter
R	Particles mean diameter
h	Vertical baffle length
s_c	Baffle column spacing
s_r	Baffle row spacing
Sr	Dimensionless parameters, $Sr = s_r / R$
Sc	Dimensionless parameters, $Sc = s_c / R$
Sc^*	$Sc^* = Sc \cdot R \cdot rh$
Sr^*	$Sr^* = Sr \cdot R \cdot rh$
R_{n1}	Baffle numbers in first row of arrays
R_{n2}	Baffle numbers in second row of arrays
R_{n3}	Baffle numbers in third row of arrays
\hat{c}_s	Sound velocity
\hat{L}	Length of simulated region
$\Delta \hat{x}$	Length step
$\Delta \hat{t}$	Time step
$\hat{\rho}$	Density

1 Introduction

Rock avalanches are a global pan-genetic mountain disaster, with hidden locations, sudden instability damage, and catastrophic consequences. It is a common sudden major geological safety hazard occurring in mountainous towns and highway transportation construction (Bi et al. 2016a; Bi et al. 2018). Wen et al. (2004) analyzed the occurrence

conditions and causes of more than 70 large-scale high-velocity rock avalanches that have occurred in China since 1990. Huang et al. (2008) investigated and analyzed landslide and rock avalanches' occurrence and distribution characteristics induced by the 5.12 Wenchuan Earthquake. At present, disaster prevention and mitigation and emergency avoidance for sudden rock avalanches meet the engineering needs of the southwest region. In addition, it is also an important goal to optimize the structure of the disaster protection system for rock avalanches in the project. At present, researchers have carried out extensive research on the protection structure for rock avalanches mainly from two aspects, i.e. physical model test and numerical simulation.

In terms of physical model tests, Zanuttigh and Paolo (2006) used two kinds of dry sand mixtures with different particle sizes to impact four different shapes of protection structures, and analyzed the dynamic impact of particles on the structure. The expansion and shape of the particle deposition area were used to determine the efficiency of structural blocking. Hauksson et al. (2007) used particle flow to simulate the impact of avalanche disaster on the square and circular baffles, and explored the influence of baffle type, baffle height, and baffle width on fluid. Jiang et al. (2013) carried out a series of studies on the impact of rock avalanches on rigid retaining walls. By changing the slope angle, slope surface friction, slope length, particle properties and other factors, they revealed the impact and deposition mechanisms of rock avalanches in the impact process. Ng et al. (2014) and Choi et al. (2014) used staggered array of baffles to study the interaction between particle flow and array of baffles structure through laboratory experiments, and discussed the energy consumption mechanism of array of baffles and the effects of array of baffles layout changes on particle flow motion status and the downstream deposition distance. Choi et al. (2017) compared the impact of vertical and curved barriers on the impact force, rising height and motion path of particle flow under different dynamic conditions ($Fr=4.7$ and 6.4).

In terms of numerical simulation, Salciarini et al. (2010) used the discrete element method (DEM) to simulate the impact of the rock avalanches generated by the collapse on the rigid fill wall and rigid retaining wall. Huang et al. (2020) used discrete element numerical simulation to analyze the energy

consumption effect of different protection structures on rock avalanches. Taking actual disasters as an example, they inverted the influence of baffle structure on rock avalanches' motion and deposition characteristics. Bi et al. (2018) used the DEM to establish a numerical model to study the influence of the baffle protection structure (the number and spacing of baffles and rows) on the force of the rock avalanches impacting the baffle, and based on this, the array of baffles-retaining wall structure was proposed, which was of great guiding significance for the design of the protection system for rock avalanches. Bi et al. (2019a, 2019b) optimized the traditional array of baffles protection structure by adding low baffles between the array of baffles to form a speed bump. Using the numerical simulation of the DEM, the effect of the array of baffles-speed bump structure was discussed in detail from both the number of low baffles and the angle of low baffles. The results showed that the array of baffles-speed bump structure could effectively improve the energy consumption effect of the structure. Using the DEM, the influence of the layout parameters of the array of baffles on the impact force of the rock avalanches was examined. The numerical simulation could comprehensively analyze the interaction between the rock avalanches and the flow impact between the array of baffles, and study the change law of the array of baffles layout on the impact force. At present, the existing studies on the interaction between baffles and rockfalls, including experiments and simulations, are small-scale, so the results cannot reflect the influence of actual topography. In addition, when considering the effect of natural disaster prevention and control, using numerical simulation alone for design is not sufficient. It is necessary to consider various research methods to design protective measures.

When baffle protection structure is used as a disaster prevention and mitigation project for rock avalanches, it is usually located downstream of the rock avalanches' path, mostly in front of the protected area (Wang et al. 2017; Fei et al. 2020a; Fei et al. 2020b). Through physical model tests and numerical simulation studies, the baffle protection structure can disturb the fluid state of the rock avalanches. When the rock avalanches contact each row of baffles, the fluid will collide and deflect. The velocity will slow down, and then accelerate to the next row to accommodate the energy consumption of the rock avalanches. However, previous studies on protection

structures for rock avalanches mainly are focused on using only physical model tests or numerical simulation, while few studies on the array of baffles structure combining the two methods. Existing research shows that experimental research can be used as a powerful tool to verify the results of numerical simulation (Moin and Mahesh 1998). Physical model tests are used to determine the mechanical properties of numerical simulations, and then numerical simulation techniques are used to verify the reliability of physical model experiments. Therefore, the physical model test and numerical simulation of the blocking and energy consumption efficiency of the array of baffles protection structure need to be further studied. Furthermore, the authors' previous studies mainly focused on the arc-shaped baffles (Wang et al. 2020; Bi et al. 2020). However, the baffle types in practical engineering are square and cylindrical.

Compared with other traditional computational fluid dynamics (CFD) methods, the lattice Boltzmann method (LBM) has the characteristics of a mesoscopic model between the microscopic molecular dynamics model and the macroscopic continuum model. Therefore, it has the advantages of simple fluid interaction description, easy setting of complex boundaries, accessible parallel computing and easy implementation of programs. LBM has been widely regarded as an effective means to describe fluid motion and deal with engineering problems. From the perspective of non-equilibrium statistical mechanics, LBM combines the completely discrete dynamic lattice model of time, space, and velocity phase space with Boltzmann equations to describe fluid motion law without directly solving the Navier-Stokes equations. Therefore, applying LBM to the numerical simulation of geological disasters is feasible..

In this study, firstly, through the physical model test on rock avalanches, combined with the comparison of the similarity between the geological background and the model of Ermanshan rock avalanche project, a comparative study was conducted to investigate the influence of the layout parameters of array of baffles structure on the rock avalanche energy consumption. From the aspects of particle deposition range, siltation depth, displacement of the rear structure of the array of baffles, etc., the optimal layout parameters were selected, and the LBM was used to simulate the impact of rock avalanches on the array of baffles structure to further study the

influence of the layout parameters of the array of baffles structure on the energy consumption and blocking of the rock avalanches.

2 Research Background

2.1 Background information

The test platform was built in the State Key Laboratory of Chengdu University of Technology, and is composed of metal bin, chute, metal deposition platform, array of baffles protection structure and other components. The engineering case used in this test is the Ermanshan landslide occurring on July 27, 2010, in Wangong Town, Hanyuan County, Sichuan Province.

The Ermanshan landslide is located in Wangongji Town, Hanyuan County, Ya'an City, Sichuan Province. It is located in the Dagou River Basin, which is about the southeast of the Xinxian Town of Hanyuan County, and on the left bank of the Pubugou Reservoir Area of Dadu River. The mountains on both sides of the Dadu River Basin are relatively steep and belong to high-medium mountain topography. The landslide area has an altitude of 1963~850 m. The landslide area is located in the alpine valley between Sichuan and the Qinghai-Tibet Plateau (102°43'26"E, 29°18'58"N), as shown in Fig. 1 of authors' previous work (Bi et al. 2021). Mountains are high, slopes are steep, terrain height differences are large, and valley cutting is deep, which are the outstanding features of the topography of the region. There is a long and narrow ditch between the Ermanshan slide source and the town, with a slope of 30°~40°. The Ermanshan rock avalanches have a height difference of about 610 m and an impact distance of about 1370

m. According to field surveys and remote sensing images, the rock avalanches directly caused more than 20 deaths and damaged more than 350 buildings. After the rock avalanches in Ermanshan, protective measures such as drainage channels and retaining walls were built between the Wangong Town and the sliding area, as shown in Fig. 1.

In the Ermanshan landslide source area, the slope top elevation is 1630 m, the deposition front elevation is 950 m, the vertical height difference is 680 m, and the horizontal distance is 1600 m. Especially in the slid source area and nearby active areas, the slope in the ditch is steep and the basalt mountain mass is prominent, with good air conditions. There are large grooves in the area. The elevation of 1025~1270 m is the deep section of early landslide and rock avalanche deposition, which provides a free surface for the motion of loose bodies at high altitudes. Once the loose bodies at the slope toe slide, it provides good air conditions for the



Fig. 1 The geomorphology and engineer layout of Ermanshan landslide (From Google Earth) in Wangongji Town, Hanyuan County, Ya'an City, Sichuan Province.

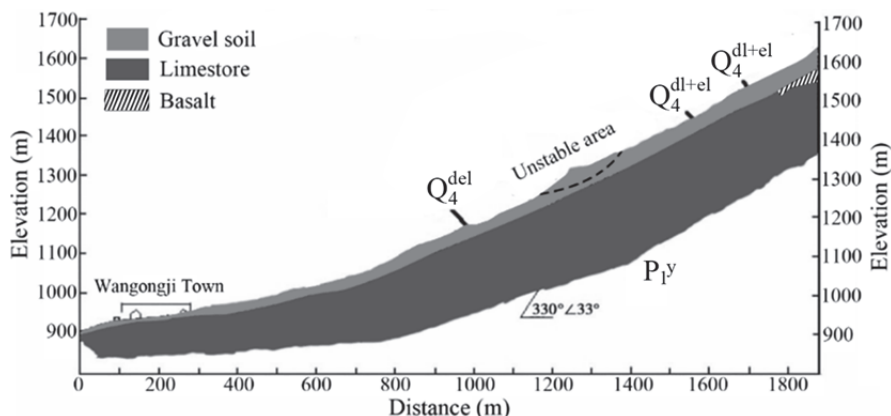


Fig 2 Profile of Ermanshan landslide in Wangongji Town, Hanyuan County, Ya'an City, Sichuan Province, China.

instability and failure of the basalt body, as shown in Fig. 2.

Due to heavy rains or showers in this area, high reclamation rate, poor vegetation coverage, rich original deposits, there are developed ancient landslides and early rock avalanches in this area. At the same time, the left side of Dagou has limestone overlying residual soil with a thickness of 5 m to 7 m. The rock tends to topple to the ditch and easily slide in the ditch along the boundary line of the base cover.

The base rock in the studied area of the landslide was composed of limestone of the Upper Permian Emeishan Basalt Formation (P₂β) and the Lower Permian Yangxin Formation (P₁γ). The surface rock mass was strongly weathered and unloaded in fragments. The geological conditions were relatively simple. There were no large-scale faults and folds in the landslide area and its surrounding areas. The high and steep slopes and deep-cut large grooves provided favorable topographical conditions for the Ermanshan rock avalanches. The abundant quaternary loose deposits provided provenance conditions for the motion of the rock avalanches. The forward slope of limestone and the columnar joints of basalt provided an advantageous slope structure for the further development of the rock avalanches. The landslide was triggered by heavy rainfall and it descended at a high velocity.

After the Ermanshan rock avalanches occurred, in order to prevent the remaining potential sources in the margin area from sliding again, a protective baffle project was built between the Wangong Town and the sliding area. Ermanshan is located in the transition zone between the Sichuan Basin and the Qinghai-Tibet Plateau. It belongs to the middle-high mountain topography with structural denudation. It is a ubiquitous topography and landform in southwestern China. Therefore, the Ermanshan rock avalanches were taken as a model to investigate its protection and blocking effects, which is of great theoretical and practical significance for the protection against high-velocity and long-distance rock avalanches. Besides, it also provides a theoretical basis for similar geological disaster prevention and control work in southwestern China.

2.2 Research assumption

Rock avalanches are usually recognized as mainly dry phenomena (Hung et al. 2001) during studies.

Some researchers (Manzella and Labiouse 2009) use small bricks to investigate parameters and mechanisms involved in rock avalanches. Some researchers (Zhao et al. 2017) use DEM method (without coupling) to study the rock fragmentation during rock avalanches. However, water content is the key factor which can accelerate rock mass dilation and fragmentation, and a successive increase in mobility of avalanches. Abele (1997) proposed a mechanism whereby a combined movement of a avalanches riding on water-saturated silt, sand, and gravel can increase both run-out distance and the spreading of the debris. There are primarily two ways for avalanches acquire water: (1) The strong rainfall can make rock avalanches become debris flow, for example, rock avalanches in Madaling gully, China, is a typical characteristic of that forming debris flow (Qi et al. 2016); (2) On a typical rock avalanche path, significant water can come in association with saturated soil entrained from the path downslope of the toe of the rupture surface (Hung et al. 2004). Thus, water content is a variable during the rock avalanches movement. It is hard to consider the water as a parameter in experiment. For this reason, two extreme conditions were designed to investigate the baffles' effect as follows: (1) assume that rock avalanches are dry granular flow; (2) assume that rock avalanches are fluid. We were planning to use physical models to study these two cases. However, it is hard to use the SFFMS (surface flow field measurement system) to get the pure fluid velocity for the SFFMS's working mechanism (Wang et al. 2020). In order to solve this problem, physical and numerical experiments are all adopted in this study.

3 Physical Model Test and Results

3.1 Physical model and similarity ratio

The test platform was composed of a metal bin, a chute, a metal deposition platform, array of baffles protection structure and other components (Fig. 3). The detailed introduction of the device can be found in authors' previous researches (Wang et al. 2020; Bi et al. 2020). The source area consisted of a rectangular metal bin with a length of 0.4 m, a width of 0.3 m, and a height of 0.9 m. The inclination angle of the circulation area in the physical model test was 35°. The circulation area consisted of a chute with a

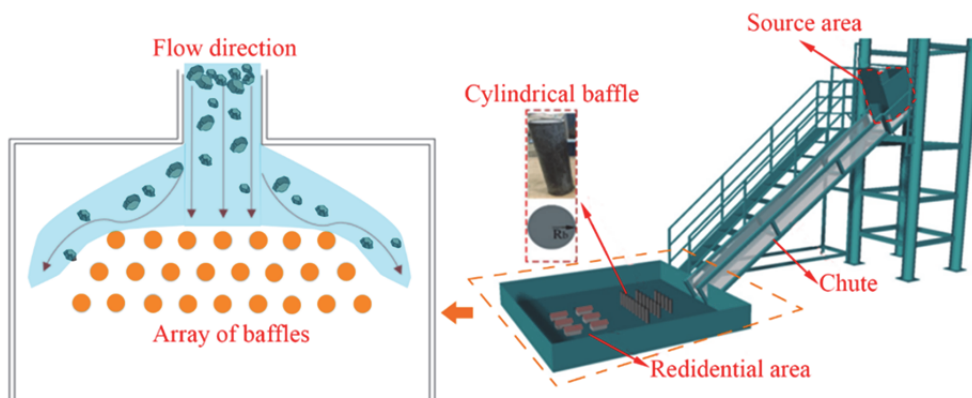


Fig. 3 Indoor test model of rock avalanches-array of baffles-disaster bearing body.

length of 4.2 m, a width of 0.3 m, and a side wall of 0.5 m high. The deposition area was a square metal platform 2.5 m long and 2.5 m wide.

During the experiment, three digital cameras were used to capture the images of fluid motion. Three cameras synchronously recorded the impact process of the test, and used the frame-by-frame video analysis method to obtain the frontal velocity of particles. A 3D laser scanner was used to scan the particle deposition morphology, and measure the deposition plane, so as to obtain the morphological characteristics of the particle deposition (maximum length, maximum width, maximum depth, deposition map and longitudinal section view).

Three similarities are required to establish a model for rock avalanches array of baffles, namely geometric similarity, motion similarity and dynamic similarity. Mass motion is related to boundary conditions and forces. Dynamic similarity and geometric similarity are basic parameters. The geometric similarity was obtained by normalizing the size of the model. The average slope of the test groove is similar to that of the channel rock avalanches of the Ermanshan landslide. The motion similarity describes the impedance generated by the interaction between the baffle and the particles, which is unknown and will be tested in this study. Gravity is the main driving force of the rock avalanches' motion, so Froude number was used to investigate the dynamic similarity between the physical model and the actual working conditions. Fr is the ratio of inertial force to gravity, which controls the similarity of force in the gravity-driven flow in the groove. In order to carry out the model experiment reasonably, we have adopted some similar methods.

The model and prototype are denoted by subscript letters m and p, respectively. Under the

same circumstance of fluids, height above sea level and the gravitational acceleration. Motion and dynamics are similar:

$$(Fr)_m = (Fr)_p = \frac{v_m}{\sqrt{gh_m}} = \frac{v_p}{\sqrt{gh_p}} \quad (1)$$

where $(Fr)_m$ and $(Fr)_p$ are the model Froude number and the prototype Froude number, respectively; v is the fluid faucet velocity; g is the gravity acceleration; h is the fluid depth;

In the dimensionless equation, the dimensionless number $(Fr)_p$ is equal to $(Fr)_m$; assuming that the experimental model and the prototype are in the same gravitational field, Fr can be combined with geometric similarity to calculate the velocity scale and flow depth scale. The Fr_{max} of the physical model test in the laboratory is about 6.4, which is equivalent to a prototype rock avalanches event with a velocity close to 24.5 m/s and a flow depth of about 1.5 m. In terms of fluid velocity, it is similar to the motion velocity of the Ermanshan rock avalanches.

$$(Fr)_m = (Fr)_p = 6.4 \quad (2)$$

$$\gamma_v = \frac{v_p}{v_m} = 5.7 \quad (3)$$

where γ_v is the fluid velocity similarity ratio; v_p is the prototype fluid velocity; v_m is the model fluid velocity;

Geometric similarity:

$$\gamma_h = \frac{h_p}{h_m} = \gamma_v^2 = 33.3 \quad (4)$$

where γ_h is the fluid depth similarity ratio; h_p is the prototype fluid depth; h_m is the model fluid depth.

3.2 Test parameters

The particle grading of the rock avalanches in the test was obtained after sampling and sieving the

actual particles of the Ermanshan rock avalanches, as shown in Fig. 4. Due to the limitation of the test site, the size ratio of the array of baffles model and the test variable parameters, the particle size range used in the test was selected to be 0.1~30 mm, the average particle size R was 2.04 cm, and the total weight was 60 kg. According to the particle size, some stones were dyed to better capture the motion trajectory of the stones.

The type of baffle used in this research was circular baffle. The radius R_b of the circular baffle was 2.5 cm, as shown in Fig. 3. The height of the protection structure was an important factor to prevent supercritical overflow. The test focused on the effect of changes in the protection structure of the array of baffles on the final deposition of rock avalanches. In order to simplify the problem, it was assumed that the height of the baffle was high enough and the baffle height was all designed to be 18 cm, which was twice the maximum stack height (9 cm) of the unobstructed control test. The main geometric parameters in the experiment are shown in Fig. 2 and Table 1.

In order to determine the optimal layout conditions, the physical model test used the optimized protection structure for rock avalanches to study its main parameters (row spacing, column spacing, number of baffles) in detail. In actual engineering, the adjustment of these three parameters is usually considered as a feasible method to increase the energy consumption of the protection system. Therefore, the following research mainly focuses on the above-mentioned main parameters. Table 2 lists the three main dimensionless parameters.

3.3 Result analysis

The studies in this paper are different from the authors' previous studies. Studies in Wang et al. (2020) and Bi et al. (2020) are mainly focused on arc-shaped baffles, while this paper mainly studies the traditional cylindrical baffles and its energy dissipation mechanism. It has been proved by authors' previous studies (Wang et al. 2020; Bi et al. 2020) that arc-shaped baffle is the best case among the three types of baffles (square baffles, cylindrical baffles, and arc-shaped baffles), however, it is usually using the cylindrical baffles and square baffles in practical engineering problems (Bi et al. 2020). Authors have also studied the dynamic response when

rock avalanches impact the single cylindrical structure and square structure (Bi et al. 2017). It has showed that the maximum impact force of rock avalanches exerted on cylindrical structure is smaller than square structure's, and the same rule is between the average impact force and two structures. For the reasons given above, the cylindrical baffles were selected in this study.

From our previous studies (Fig. 7 in (Bi et al. 2021)), it has showed the deposition result of the impact test without a protection structure. The

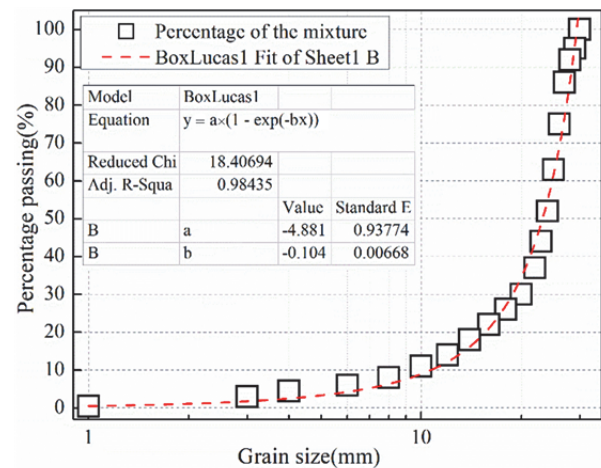


Fig. 4 Particle grading curve of the rock avalanches in the test.

Table 1 Geometric parameters of the test

Description	Symbol	Value
Slope angle (°)	α	35.0
Slope length 1 (cm)	$Ls1$	4.2
Slope length 2 (cm)	$Ls2$	80.0
Length of Row 1 (cm)	m_1	65
Length of Row 2 (cm)	m_2	75
Length of Row 3 (cm)	m_3	85
Baffle diameter (cm)	r	5
Particles mean diameter (cm)	R	2
Vertical baffle length (cm)	h	18.0
Baffle column spacing (cm)	s_c	3, 5, 7, 9, 11
Baffle row spacing (cm)	s_r	5, 7, 9, 11

Table 2 Dimensionless variable parameters in the experiment

Case number	$Sr = s_r / R$	$Sc = s_c / R$	Baffle row's number
1	4.5	1.5	1,2,3
2	4.5	2.5	1,2,3
3	4.5	3.5	1,2,3
4	4.5	4.5	1,2,3
5	4.5	5.5	1,2,3
6	2.5	3.5	1,2,3
7	3.5	3.5	1,2,3
8	4.5	3.5	1,2,3
9	5.5	3.5	1,2,3

deposition range was 70~205 cm. The maximum depth of fluid deposition was 9 cm, and the maximum width of the deposition was 118 cm. The deposition area was 11477.5 cm².

Increasing the number of baffles can effectively reduce the frontal velocity and deposition range of the rock avalanches (Ng et al. 2015). In this experiment, the 5th to 8th case of experiments also proved this phenomenon. The impact results of different numbers of baffle rows are shown in Fig. 5. In Fig. 5(a), the deposition areas of one, two, and three rows of baffles were 7994 cm², 7802 cm², and 7535 cm², respectively. The deposition area of three rows of baffles was smaller than that of one row of baffles and that of two

rows of baffles. The deposition area was reduced by 2.4% and 5.7%, respectively. With the increase of the number of baffles, the deposition width of the rock avalanches increased, the impact distance decreased, and the range of movement of the rock avalanches could be effectively suppressed.

In Fig. 5(b) and Fig. 5(c), the maximum deposition thickness of one, two, and three rows of baffles were 11.6 cm, 11.8 cm, and 12.4 cm, respectively. As the number of baffles increased, the deposition depth of particles increased accordingly.

It can be seen from Fig. 5 that when one or two rows of baffles were arranged, some particles were deposited behind the baffles after being impacted by the rock avalanches. Three rows of baffles were arranged, and most of the particles were blocked in the baffles, while, only a small number of particles caused by splashing and jumping had passed. However, increasing the number of baffles could not solve this problem well. From the comprehensive comparison of particle deposition area and deposition thickness, a three-row array of baffles layout was adopted to prevent the rock avalanches.

Under the condition of row spacing $Sr=4.5$, the deposit results of three rows of array of baffles with different column spacing were compared, as shown in Fig. 6. In Fig. 6(a), the deposition areas of $Sc=2.5, 3.5, 4.5, 5.5$ were 7535 cm², 7659 cm², 7921 cm², 8035 cm², respectively. Compared with other cases, the deposition area of $Sc=2.5$ was the smallest, and from the perspective of the deposition range, the utilization rate of the array of baffles was also higher.

In Fig. 6(b) and Fig. 6(c), the maximum siltation depth with $Sc=2.5, 3.5, 4.5, 5.5$ was 12.4 cm, 12.2 cm, 12.0 cm, and 11.7 cm, respectively. With the increase of the column spacing, the siltation depth in front of the baffles decreased, and the siltation depth of particles behind the baffles increased. When $Sc=2.5$, the siltation depth in front of the baffle was the highest; when $Sc=2.5$, the average siltation depth in front of the baffle was the lowest and the volume of blocked particles was the largest; when $Sc=5.5$, the siltation depth behind the baffle was the highest. In summary, when the Sr value was constant, $Sc=2.5$ had a better blocking effect and bounce suppression effect on the rock avalanches.

Under the condition of column spacing $Sc=2.5$, the impact results of three rows of array of baffles with different row spacing were compared, as shown in Fig. 7. It can be seen from Fig. 7(a) that with the

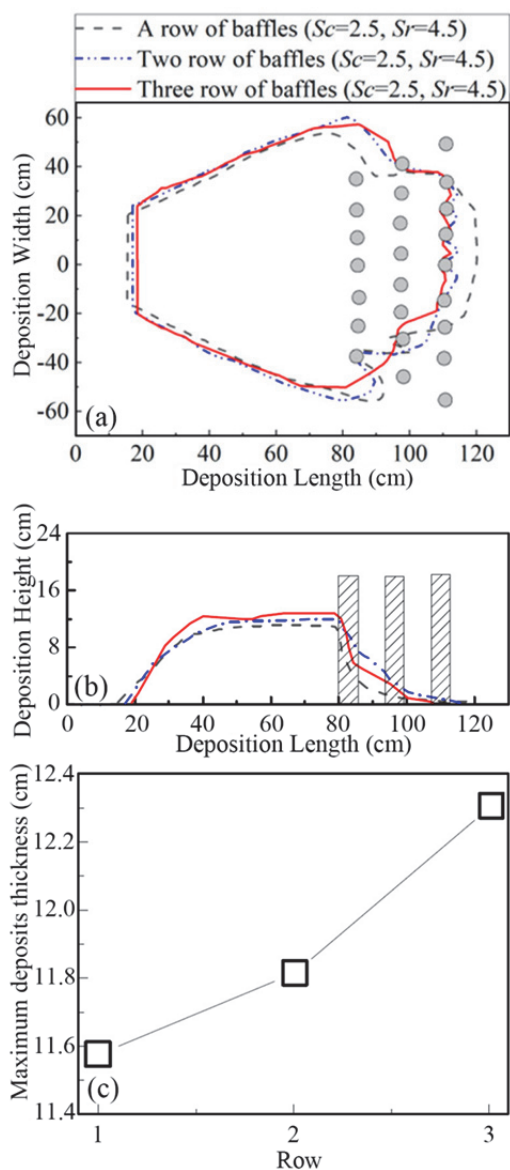


Fig. 5 Comparison of different numbers of baffle rows: (a) deposition area; (b) siltation depth; (c) maximum siltation depth.

increase of the row spacing S_r , the deposition distance of the rock avalanches gradually increased, and the number of flanking particles gradually decreased. The deposition areas of $S_r=2.5, 3.5, 4.5, 5.5$ were $8192 \text{ cm}^2, 7925.5 \text{ cm}^2, 7535 \text{ cm}^2,$ and 8612.5 cm^2 , respectively. In the case of $S_r=4.5$, the deposition area of rock avalanches was the smallest.

In Fig. 7(b) and Fig. 7(c), the maximum siltation depth with $S_r=2.5, 3.5, 4.5, 5.5$ was $12.7 \text{ cm}, 12.6 \text{ cm}, 12.4 \text{ cm},$ and 12.2 cm , respectively. As the row spacing increased, the siltation depth before and after the baffles decreased. Therefore, when $S_r=5 \text{ cm}$, the deposition depth was the largest, and when $S_r=5.5$, the deposition depth was the smallest.

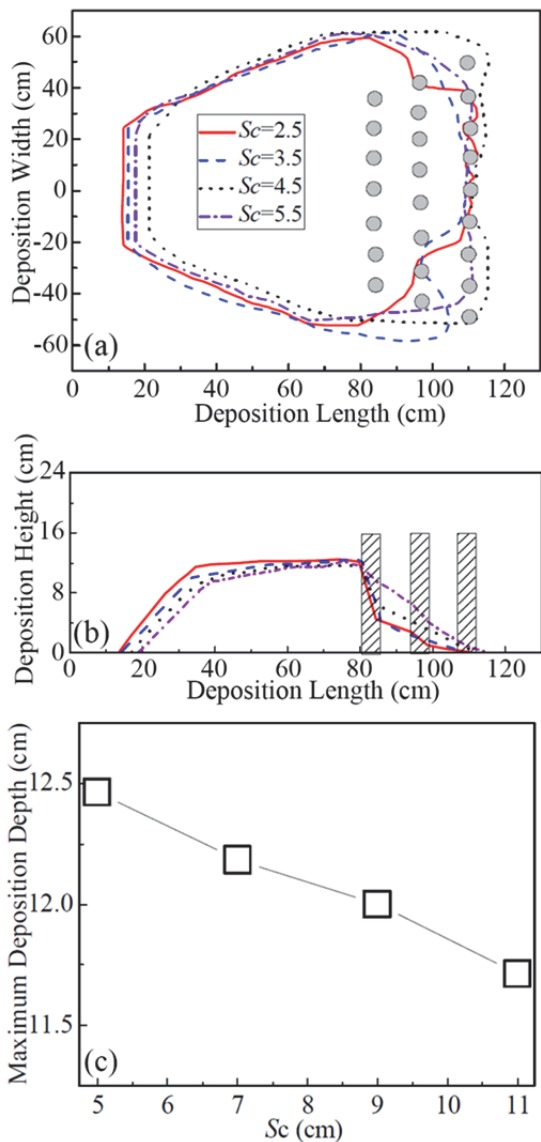


Fig. 6 Comparison of different column spacings: (a) deposition area; (b) siltation depth; (c) maximum siltation depth.

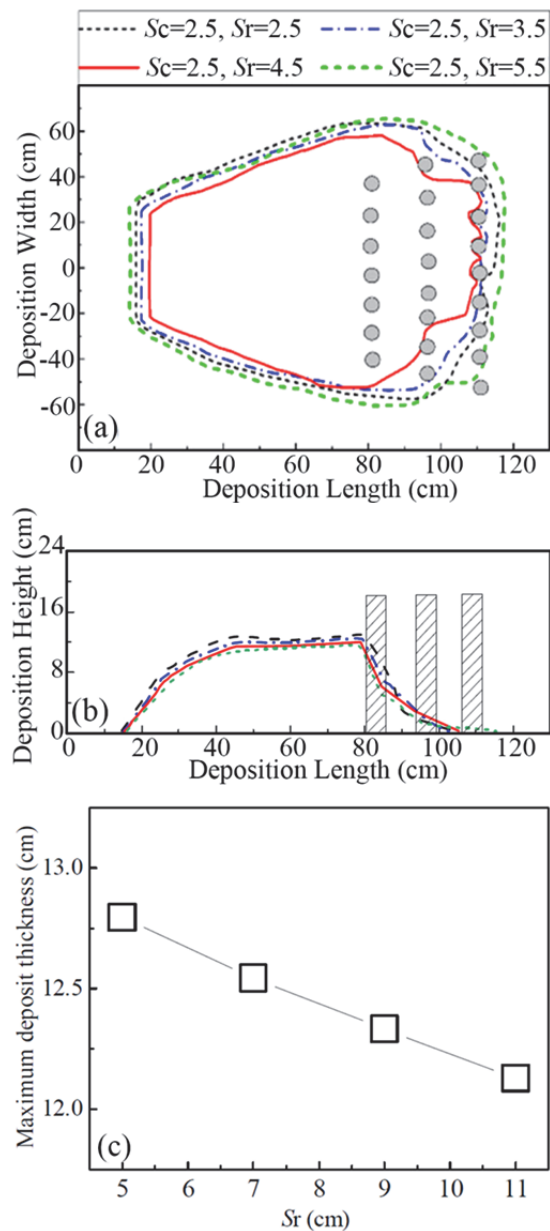


Fig. 7 Comparison of different row spacings: (a) deposition area; (b) siltation depth; (c) maximum siltation depth.

In summary, as the row spacing S_r increased, the motion path of rock avalanches increased, the fluid energy was consumed during the motion, and the blocking effect of the array of baffles increased. Combining the deposition area and siltation depth, it could be concluded that $S_r=4.5$ had a better blocking effect and bounce suppression effect for the grooved rock avalanches when the Sc value was constant.

The optimal layout parameters of circular baffles with the best blocking effect in this physical model test were three rows of array of baffles, $Sc=2.5$,

$Sr=4.5$. By restoring the similarity ratio with the actual project, in the prototype grooved rock avalanches event with a velocity close to 24.5 m/s and a flow depth of about 1.5 m, the layout parameter was the three-row circular array of baffles with $Sc^*=Sc \cdot R \cdot rh = 0.85$ m, $Sr^*= Sr \cdot R \cdot rh = 1.51$ m, which could play the role of optimizing the drainage, blocking and energy consumption performance.

The physical model test mainly considered the influences of different array of baffles layout parameters on the suppression of disaster-causing performance and energy consumption effect of the rock avalanches from the perspective of the array of baffles blocking effect, and did not deeply analyze the dynamics mechanism of the rock avalanches under the action of the array of baffles structure. Therefore, using the LBM, a numerical simulation model of rock avalanches-array of baffles-hazard-bearing body was established to analyze the impact of rock avalanches on the array of baffles. The model was also used to analyze the interaction mechanism of rock avalanches and different baffle-type structures, fluid velocity and flow direction under different layout conditions.

4 Numerical Simulation Results

4.1 LBM Introduction

Lattice Boltzmann method (LBM) is a computational fluid dynamics method of mesoscopic simulation scale. LBM uses a density distribution function to solve fluid flow and diffusion problems. The governing equation of LBM can be divided into collision part and streaming part.

$$\text{Collision step: } f_i^*(x, t) = f_i(x, t) - \Omega [f_i(x, t) - f_i^{eq}(x, t)] \quad (5)$$

$$\text{Streaming step: } f_i(x + e_i \Delta t, t + \Delta t) = f_i^*(x, t) \quad (6)$$

where $f_i(x, t)$ is the distribution function of the discrete velocity e_i of x at time t ; $f_i^{eq}(x, t)$ is the average distribution function; $f_i^*(x, t)$ is the post-collision distribution function; Ω is the collision parameter.

Depending on the values of collision parameters, LBM models can be divided into two types, i.e. Bhatnagar-Gross-Krook (BGK) model or single-relaxation-time (SRT) model (Succi et al. 2002; Ansumali et al. 2003; Huber et al. 2010; Yang et al.

2014) and multiple-relaxation-time (MRT) model (Lallemand and Luo 2000).

In this study, the MRT model was adopted due to its advantages in numerical stability, accuracy and computational efficiency. The collision algorithm of MRT is expressed as follows:

$$f_i(x + e_i \Delta t, t + \Delta t) - f_i(x, t) = -(\mathbf{M}^{-1} \mathbf{S}_f \mathbf{M}) [f_i(x, t) - f_i^{eq}(x, t)] \quad (7)$$

where \mathbf{M} is the transformation matrix; \mathbf{S}_f is the diagonal relaxation matrix. Considering the accuracy of the results, the D2Q9 discrete velocity model was used to establish a fluid dynamics model. For the D2Q9 discrete velocity model, we can define:

$$e_i = \begin{cases} (0,0) & i = 0 \\ \left\{ \cos \left[(i-1) \frac{\pi}{2} \right], \sin \left[(i-1) \frac{\pi}{2} \right] \right\} & i = 1, 2, 3, 4 \\ \sqrt{2} \left\{ \cos \left[(i-5) \frac{\pi}{2} + \frac{\pi}{4} \right], \sin \left[(i-5) \frac{\pi}{2} + \frac{\pi}{4} \right] \right\} & i = 5, 6, 7, 8 \end{cases} \quad (8)$$

$$\mathbf{M} = \begin{bmatrix} 1 & 1 & 1 & 1 & 1 & 1 & 1 & 1 & 1 \\ -4 & -1 & -1 & -1 & -1 & 2 & 2 & 2 & 2 \\ 4 & -2 & -2 & -2 & -2 & 1 & 1 & 1 & 1 \\ 0 & 1 & 0 & -1 & 0 & 1 & -1 & -1 & 1 \\ 0 & -2 & 0 & 2 & 0 & 1 & -1 & -1 & 1 \\ 0 & 0 & 1 & 0 & -1 & 1 & 1 & -1 & -1 \\ 0 & 0 & -2 & 0 & 2 & 1 & 1 & -1 & -1 \\ 0 & 1 & -1 & 1 & -1 & 0 & 0 & 0 & 0 \\ 0 & 0 & 0 & 0 & 0 & 1 & -1 & 1 & -1 \end{bmatrix} \quad (9)$$

He and Luo (1997) proposed that the average distribution function of the D2Q9 model of the incompressible N-S equation is given by:

$$f_i^{eq}(x, t) = w_i \left\{ \rho + \rho_0 \left[\frac{e_i \cdot u}{c_s^2} + \frac{(e_i \cdot u)^2}{2c_s^4} - \frac{u^2}{2c_s^2} \right] \right\} \quad (10)$$

where w_i is the weight coefficient; c_s is the lattice propagation velocity; ρ is a variable related to pressure, $p = c_s^2 \rho$, where ρ_0 represents the density of the fluid, which is constant; according to He and Luo (1997), we selected the parameters of w_i and c_s of the D2Q9 model as follows:

$$w_0 = \frac{4}{9}, w_{1-4} = \frac{1}{9}, w_{5-8} = \frac{1}{36}, c_s = \frac{1}{\sqrt{3}} \quad (11)$$

And, the relaxation matrix \mathbf{S}_f of the D2Q9 model is:

$$\mathbf{S}_f = \text{diag}(s_\rho, s_e, s_\varepsilon, s_j, s_q, s_j, s_q, s_v, s_v) \quad (12)$$

Usually, the parameters in the relaxation matrix take values between 0 and 2 (Lallemand and Luo 2000; Luo et al. 2011; Bettaibi et al. 2016; Zhou et al. 2016). The values of the relaxation parameters in Eq. (13) are as follows:

$$s_\rho = s_j = 1.0, s_e = s_\varepsilon = s_v = \frac{1}{\tau_f}, s_q = \frac{16s_v - 8}{8s_v - 1} \quad (13)$$

where τ_f is the relaxation time, which is a fixed value of 1.0 and is consistent with previous studies. In addition, through the Chapman-Enskog expansion, the relaxation rate s_v can be transformed into the macroscopic motion velocity v , and the macroscopic density and velocity can be expressed by:

$$v = c_s^2 \left(\frac{1}{s_v} - \frac{1}{2} \right) \Delta t \tag{14}$$

$$\rho = \sum_{i=0}^8 f_i(x, t) \tag{15}$$

$$\rho \mathbf{u} = \sum_{i=0}^8 f_i(x, t) \mathbf{e}_i \tag{16}$$

4.2 Boundary conditions and parameter selection

Velocity boundary conditions are usually used for entry and exit boundaries. Therefore, Zhou and He (1997) proposed the Zhou-He theory. The periodic boundary conditions used apply to the top and bottom boundaries (Succi et al. 2002). The expression equation of LBM is as follows:

$$f_{2,6,5}(i, 0) = f_{2,6,5}(i, N_y - 1) \tag{17a}$$

$$f_{4,7,8}(i, N_y) = f_{4,7,8}(i, 2) \tag{17b}$$

where N_y represents the sum of the lattice in the y direction; i represents the index in the x direction.

For the array of baffles structure, the collision rebound formula is as follows:

$$f_i(\mathbf{x}_b, t + \Delta t) = f_i^*(\mathbf{x}_b, t) \tag{18}$$

where \mathbf{x}_b is the surface lattice of the array of baffles structure, and the boundary conditions of the calculation domain are shown in Table 3.

The parameters selected in the numerical simulation are shown in Table 4.

4.3 Comparison to verify the numerical results

To determine the parameters used in the simulation experiment, a major similitude is needed

Table 4 Parameter selection for LBM method in this study

Simulation parameter	Physical quantity	Physical value	Lattice quantity	Lattice value	Transformation equation
Sound velocity	\hat{c}_s	340.40 m·s ⁻¹	c_s	1/√3	$u_r = \hat{c}_s/c_s$
Length of simulated region	\hat{L}	1.0×10 ¹ m	L	500	$L_r = \hat{L}/L$
Length step	$\Delta\hat{x}$	2.0×10 ⁻² m	Δx	1	$\partial\hat{x} = L_r \partial x$
Time step	$\Delta\hat{t}$	4.47×10 ⁻⁵ s	Δt	1	$\Delta\hat{t} = \Delta t L_r / u_r$
Density	$\hat{\rho}$	1.0×10 ³ kg·m ⁻³	ρ	1	$\hat{\rho} = \rho \Delta\hat{m} / \Delta\hat{x}^3$

for modeling the avalanche-structure interaction: velocity similarity (Li et al. 2020). In this paper, the numerical model is simplified by authors (see in Fig. 8). This is because the velocities that avalanches reach the chute’s terminal have been acquired through physical tests, which is the main influence factor affecting the accuracy of numerical simulation results. In order to justify that the parameters used in the simulation experiment are reasonable, two cases are conducted to compare the numerical and physical results. The velocity distribution of physical test is made by surface flow field measurement system developed by Yan and Cui (Institute of Mountain Hazards and Environment, CAS) (Wang et al. 2020).

Fig. 9 shows the comparison of the instantaneous velocity distribution between the physical experiment and computer simulation at different time steps under two cases situation. At $t=4.95$ s, avalanches just moved in front of the baffles; from $t=5.10$ s, avalanches begin to bypass the baffle regions in $Sc=1.5$ situation and pass the baffles regions in $Sc=3.5$ situation; from $t=5.15$ s, the rules mentioned above are

Table 3 Boundary condition setting of calculation domain

Boundary	Boundary condition	LBM equations
Entrance	Velocity boundary	Zhou-He theory
Exit	Velocity boundary	Zhou-He theory
Top	Periodic boundary	Periodic theory
Bottom	Periodic boundary	Periodic theory
Array of baffles structure	Wall	Periodic theory

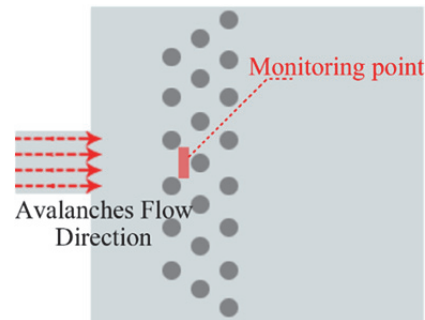


Fig. 8 Diagram of the detail position of monitoring point.

more obvious. When the $Sc=1.5$ and $t=5.2$ s, velocity clouds are distributed around the baffles, more avalanches tend to bypass the baffle region; while when the $Sc=3.5$ and $t=5.2$ s, velocity clouds are distributed between the baffles' gaps, more avalanches tend to pass the baffle region. This is because a reduction in baffle density will decrease the extent of fragment blockage; subsequent avalanches will cross baffles region easier at lower baffle density than when baffle density is greater.

For a more detailed comparison, a monitoring point was set between the first baffle row and the second baffle row (Fig. 8), which used to monitor the velocity variation at this point both in the numerical and physical test. Fig. 9 shows that the velocity variation under different column spacing in the monitoring point. As illustrated in Fig. 10, the measured data in each point is nearly equal to the calculated data. Furthermore, both the experiments share a similar velocity changing trend. The velocity value of computed data is much higher than measured data at 7.0 s in Fig. 10(a), whereas, the computed data is almost same with the measured data in Fig. 10(b). This may be because the value of Sc in Fig. 10(a) is only 1.5, which will make the blockage in baffles' gap in physical experiments (the subsident particles decelerated). As the numerical methods didn't consider the blockage situation (for the reason of continuous mechanics method), the baffles' blockage didn't happen in computed cases. Furthermore, as Sc increase, the influence of baffles' blockage decrease, which make the velocity value of measured data nearly same with the computed data in Fig. 10(b).

5 LBM For Further Study and Result Analysis

As the physical results show that $Sc=2.5$, $Sr=4.5$ is the best way for baffle configuration, however, the internal mechanism is not clear and needs to be explored. A comparison between the experimental and the numerical velocity results showed that LBM could be used instead of the physical experiment to some extent. Some elements in physical model such as baffle densities are difficult to control, moreover, some parameters in physical experiment such as velocities are hard to test. Therefore, it is preferable to use a numerical experiment to investigate the velocity

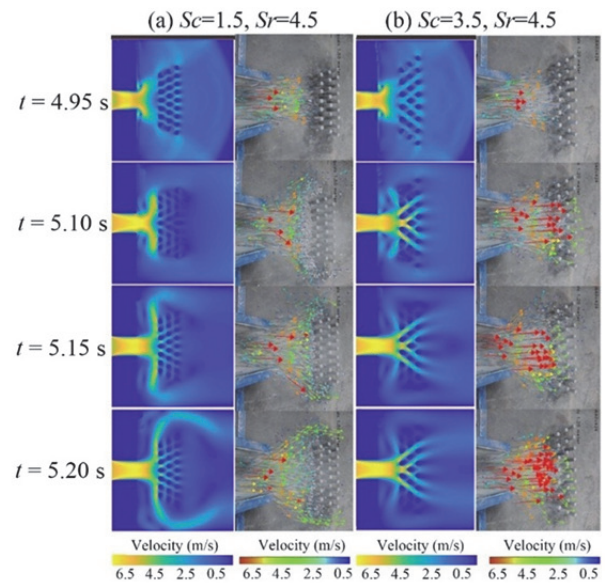


Fig. 9 Flow-obstacle interaction: comparison between laboratory experiment and LBM simulation.

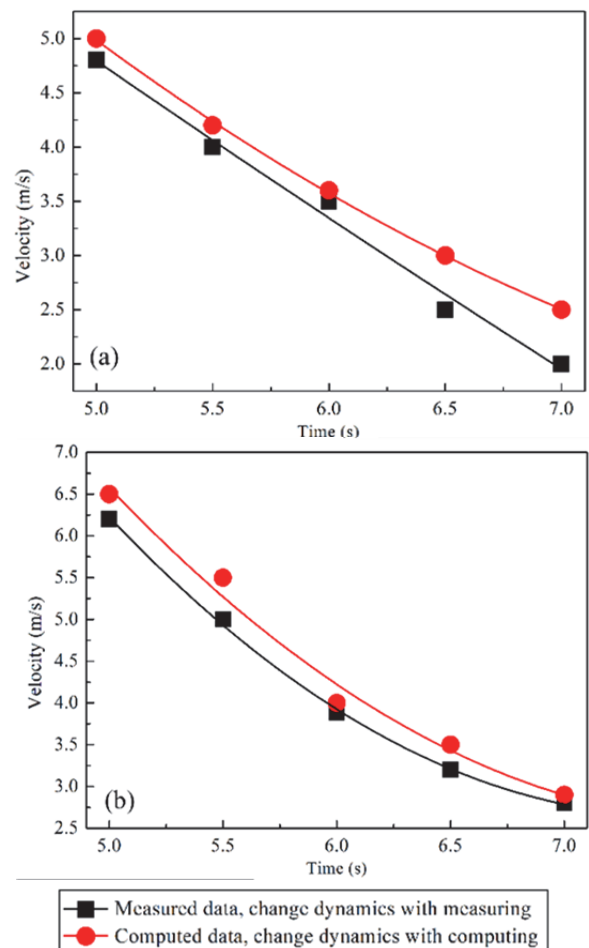


Fig. 10 Relationship between velocities in monitoring point and time steps under different column spacing conditions.

evolution principle of avalanches under different baffles configuration cases.

5.1 Influence of column spacing on the flow velocity (variable column spacing)

In order to quantitatively describe the deceleration effect of the array of baffles on the rock avalanches under different experimental conditions, the velocity attenuation ratio was adopted (Wang 2017):

$$v' = \frac{v_0 - v_t}{v_0} \tag{20}$$

where v_0 is the velocity of the rock avalanches from the flow area to the entrance of the deposition area; v_t is the instantaneous velocity of the rock avalanches impacting the array of baffles structure at time t .

Table 5, Fig. 11 and Fig. 12 show the comparison of the impact results of three rows of array of baffles with different column spacings under the condition of row spacing $S_r=4.5$. Fig. 11(a)- Fig. 11(c) present the velocity attenuation diagram at the first, second and third row of baffles, respectively.

Table 5 Velocity changes under different column spacings

Sc	First row		Second row		Third row	
	V_{max} (m/s)	\bar{V} (m/s)	V_{max} (m/s)	\bar{V} (m/s)	V_{max} (m/s)	\bar{V} (m/s)
0.5	0.84	0.4	1.34	0.2	1.7	0.3
1.5	2.27	2.0	2.50	1.6	2.26	1.2
2.5	3.47	3.1	3.09	2.3	2.61	2.0
3.5	5.08	4.4	3.03	2.4	2.76	1.9
4.5	5.90	4.9	3.15	2.7	2.77	2.0

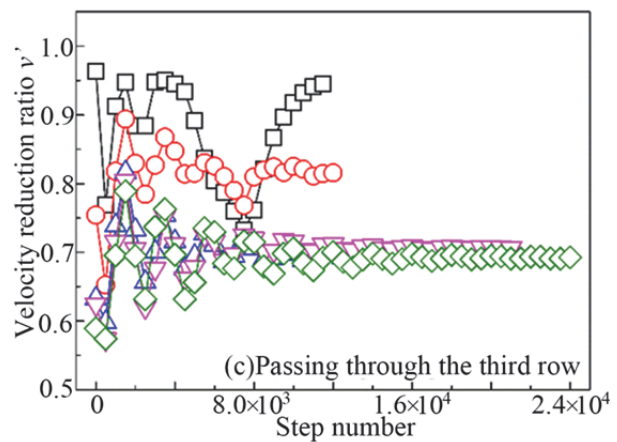
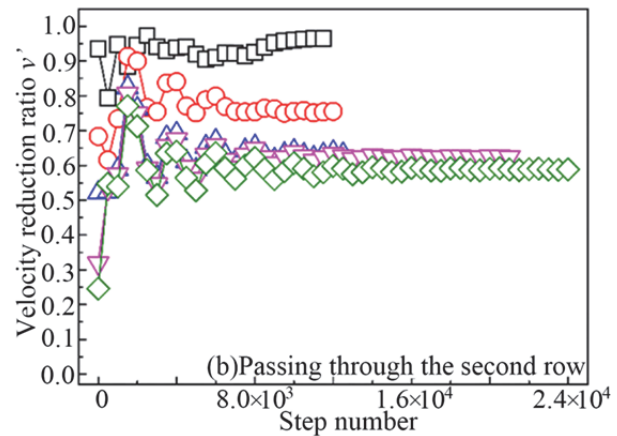
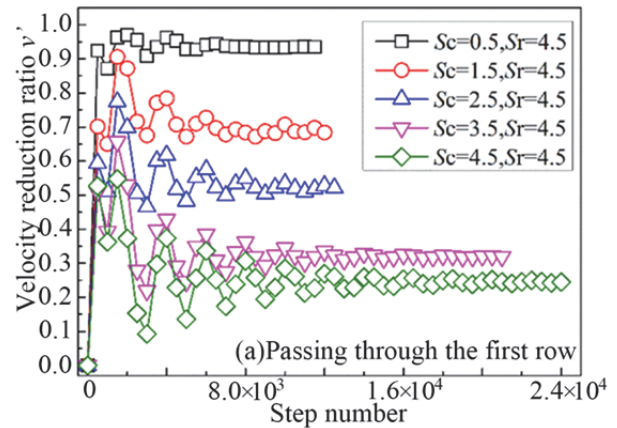


Fig. 11 The influence of column spacing on fluid velocity.

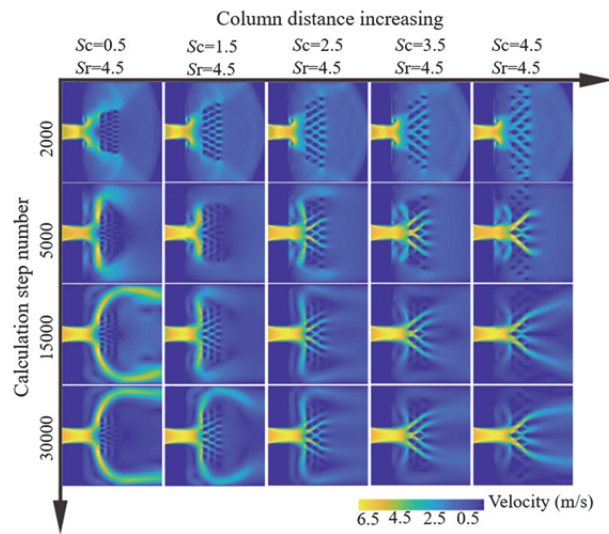


Fig. 12 Velocity flow field diagram with column spacing changing.

The maximum velocity V_{max} and average velocity \bar{V} of the rock avalanches through the first row of array of baffles are shown in Table 5. Under the working conditions of $Sc=0.5, 1.5, 2.5, 3.5, 4.5$, the velocity of the rock avalanches when it reached the first row of baffles was 93.5%, 68.3%, 52.2%, 31.9%, and 24.6% lower than that under the condition of no

baffles. The velocity of the rock avalanches when it reached the second row of baffles was 96.4%, 75.5%, 63.3%, 62.4%, and 58.9% lower than that under the condition of no baffles. The velocity when the flow reached the third row of baffles was 94.5%, 81.6%, 69.9%, 70.4%, and 69.2% lower than that under the condition of no baffles. Under different Sc conditions, the velocity attenuation rate increments from the first row to the third row were 1%, 13.3%, 17.7%, 38.5%, and 44.6%, respectively. It can be seen from the data that when $Sc=0.5$, the first row of array of baffles caused most of the kinetic energy loss to the rock avalanches, but the second and third rows of array of baffles had little effect on blocking and energy consumption of rock avalanches. Under the three working conditions of $Sc=2.5$, 3.5 and 4.5, the third row of baffles had almost the same loss of fluid velocity, but the first row of baffles under $Sc=2.5$ had the largest loss of rock avalanches velocity. Therefore, with the column spacing Sc increasing, the velocity of the rock avalanches through the first row of baffles gradually increased, and the energy consumption effect of the back row of baffles on the rock avalanches became more obvious.

It can be seen from the velocity attenuation rate curve in the figure that when the rock avalanches contacted the array of baffles, its flow state and motion trajectory were disordered, and the particles would deflect, collide, and jump, causing fluid energy loss. Therefore, the velocity dropped sharply. However, with the subsequent impact of the rock avalanches, the particle velocity immediately started to increase after a sharp drop, reaching the maximum velocity through the first row of baffles. Each velocity fluctuation showed the rapid energy loss of the rock avalanches in the high-velocity flow state. After the turbulent period in the state of high kinetic energy, as the velocity of the rock avalanches decreased, the velocity fluctuations caused by the fluid's colliding with the array of baffles structure gradually decreased, and began to pass through the first row of baffles in a relatively stable state. The flow state had entered a stable period. However, in Fig. 11(c), when the baffles were relatively dense, for example, when $Sc=0.5$, the velocity of rock avalanches would suddenly increase up to 1.74 m/s. This was because the rock avalanches flowing around the two sides of the protection structure reached the third row of baffles, causing the velocity of the rock avalanches at the end of the baffle to increase. This also showed that

although reducing the column spacing could effectively reduce the rock avalanches velocity through the array of baffles, the rock avalanches passing through the two sides increased, and the overall protection effect was weakened. Only a moderate increase in the array of baffles density could achieve the optimal effect of reducing the kinetic energy of rock avalanches. Under the conditions of $Sc=0.5$ and 1.5, the rock avalanches had a certain degree of circumfluence. Under the condition of $Sc=0.5$, the velocity of the fluid affected by the circumfluence when reaching the third row of baffles was increased by 480% than the average velocity. Under the condition of $Sc=1.5$, the velocity of the fluid affected by the flow around the third row of baffles increased by 25.4% compared to the average velocity. Under the conditions of $Sc=2.5$, 3.5, 4.5, the velocity did not change abnormally. It can be seen that the baffle density interfered with the flow state of rock avalanches.

It can be seen from Fig. 12 that when $Sc=0.5$ and 1.5, after the rock avalanches impacted the array of baffles protection structure, the rock avalanches moved to both sides of the array of baffles at a higher velocity, and there were almost no particles in the array of baffles structure. Therefore, the structure of the first row of array of baffles would bear most of the impact of rock avalanches, while the second and third rows almost played no role. The utilization rate of the array of baffles protection structure under this parameter was extremely low. The energy consumption and blocking effect of rock avalanches was extremely poor. When $Sc=2.5$, a small number of particles moved to both sides of the array of baffles, and most of the rock avalanches passed through the energy consumption and barriers of the three-row array of baffles protection structure, and finally stayed within the protection range of the array of baffles structure. When $Sc=3.5$ and 4.5, almost no particles passed through the two sides of the array of baffles structure, but because the column spacing was too large, a large number of particles passed through the array of baffles, posing a threat to the protected area behind. In summary, when the Sr value was constant, $Sc=2.5$ had a better blocking effect and velocity suppression effect on the rock avalanches.

5.2 Influence of row spacing on flow velocity (variable row column spacing)

Table 6 Velocity changes under different row spacings

Sr	First row		Second row		Third row	
	V_{max} (m/s)	\bar{V} (m/s)	V_{max} (m/s)	\bar{V} (m/s)	V_{max} (m/s)	\bar{V} (m/s)
2.5	2.53	1.6	2.55	1.4	2.45	1.3
3.5	2.69	2.4	3.10	2.2	2.73	1.9
4.5	3.47	3.1	3.09	2.3	2.61	2.0
5.5	4.90	4.2	2.96	2.3	2.61	2.0

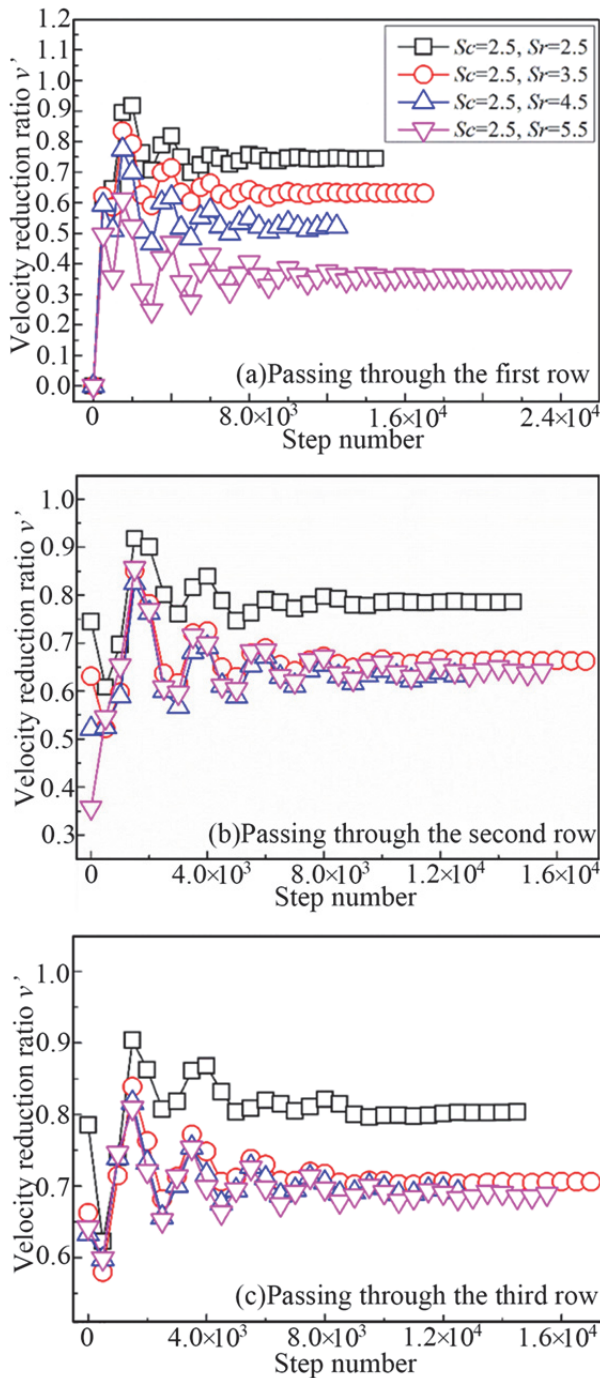


Fig. 13 Effect of row spacing on fluid velocity.

Table 6, Fig. 13 and Fig. 14 show the comparison of the impact results of three rows of array of baffles with different row spacings under the condition of column spacing $S_c=2.5$. Fig. 13(a)-Fig. 13(c) present the velocity change graph at the first, second and third rows of array of baffles, respectively.

The maximum velocity V_{max} and average velocity \bar{V} of the rock avalanches passing through the array of baffles are shown in Table 6. Under the conditions of $Sr=2.5, 3.5, 4.5, 5.5$, the velocity of the rock avalanches when it reached the first row of baffles was 74.5%, 63.1%, 52.2%, and 35.7% respectively lower than that under the condition of no baffles. When the rock avalanches reached the second row of baffles, the velocity of the rock avalanches was reduced by 78.6%, 66.3%, 63.3%, and 64.2%, respectively. When the rock avalanches reached the third row of baffles, the velocity was reduced by 80.3%, 70.6%, 69.9%, and 68.9%, respectively, compared with the velocity of the rock avalanches under the condition of no array of baffles. Therefore, under different Sr conditions, the velocity attenuation rate increments from the first row to the third row were 5.8%, 7.5%, 17.7%, and 33.2%, respectively. It can be seen from the data that when $Sr=2.5$, the array of baffles had the best energy consumption effect on the rock avalanches, but as the row spacing Sr increased, the velocity of the rock avalanches passing through the first row of array of baffles gradually increased, and the energy consumption effect of the rear baffles on the rock

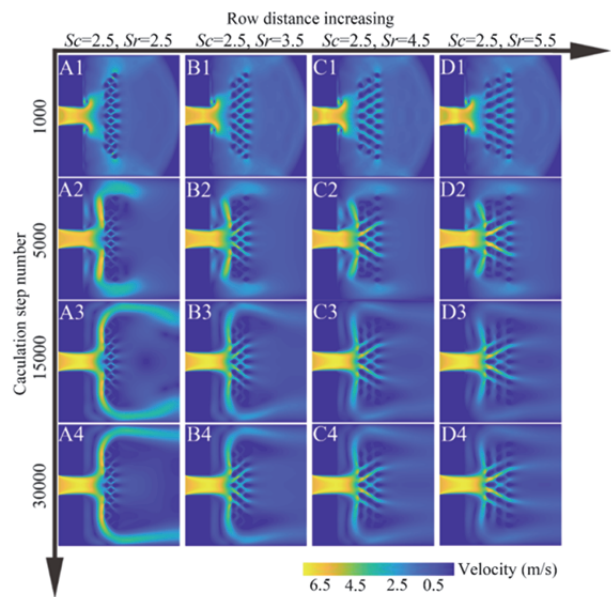


Fig. 14 Velocity flow field diagram with row spacing changing.

avalanches got more obvious.

It can be seen from Fig. 14 that when $Sr=2.5$, the rock avalanches impacted the array of baffles protection structure and then blocked, the motion direction of the rock avalanches was mainly to the two sides of the array of baffles, and a very small number of particles entered the array of baffles structure. The utilization rate of the array of baffles protection structure under these parameters was extremely low, and the drainage and energy consumption effect of rock avalanches was extremely poor. As Sr increased,

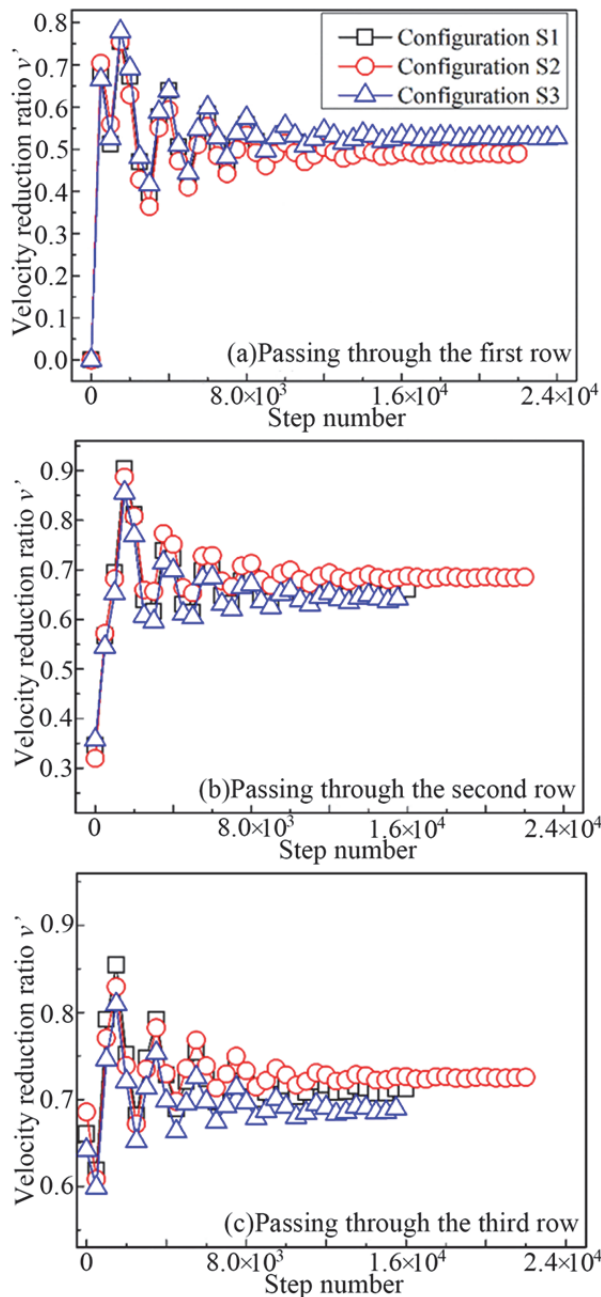


Fig. 15 Influence of the number of baffles on the fluid velocity.

the blocking effect of the array of baffles weakened, and a large number of particles passed through the array of baffles structure. When $Sr=3.5$, a small number of particles moved to both sides of the array of baffles, and most of the rock avalanches finally stayed within the range of the array of baffles structure due to the energy consumption and blocking effects of the three-row array of baffles protection structure. When $Sr=4.5$ and 5.5 , almost no particles passed through the two sides of the array of baffles structure, but because the column spacing was too large, a large number of particles passed through the array of baffles, posing a threat to the protected area behind. In summary, $Sr=3.5$ had a better blocking effect and drainage effect on rock avalanches.

5.3 Influence of the number of baffles on the flow velocity

The number of baffles is also an important indicator to measure the application value of a protection project. Therefore, this simulation only used three kinds of the layout of array of baffles (S1, S2, S3) for comparative study. S1 arrangement was $R_{n1}=5, R_{n2}=6, R_{n3}=7$, a total of 18 baffles; S2 arrangement was $R_{n1}=6, R_{n2}=7, R_{n3}=8$, a total of 21 baffles; S3 arrangement was $R_{n1}=7, R_{n2}=8, R_{n3}=9$, a

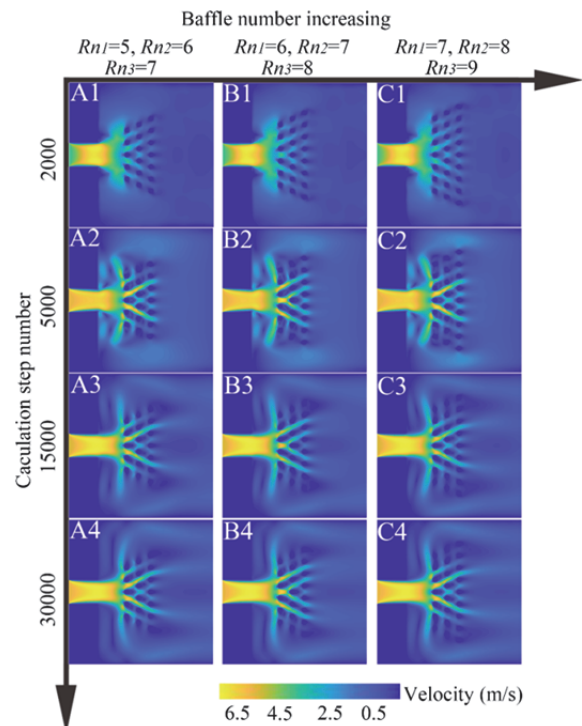


Fig. 16 Velocity flow field diagram with number of baffles changing.

total of 24 baffles. Fig. 15 and Fig. 16 show the comparison of the impact results of three-row array of baffles with different row spacings under the condition of column spacing $Sc=2.5$. Fig. 15(a)-Fig. 15(c) present the velocity change graphs at the first, second and third rows of array of baffles, respectively.

The maximum velocity V_{max} and average velocity \bar{V} of the rock avalanches passing through the array of baffles are shown in Table 7. Under the S1, S2, and S3 working conditions, the velocity of the rock avalanches when it reached the first row of baffles was 51.7%, 49.6%, and 52.7% lower than that under the condition of no array of baffles. the velocity of the rock avalanches when it reached the second row was 64.2%, 65.6%, and 63.3% lower than the velocity of the rock avalanches under the condition of no array of baffles. The velocity of the rock avalanches reaching the third row of array of baffles was higher than that of the rock avalanches under the condition of no array of baffles. The rate of the rock avalanches was reduced by 71.6%, 72.2%, and 69.9% respectively. Therefore, under different Sr conditions, the velocity attenuation changes from the first row to the third row were 19.9%, 22.6%, and 16.7%, respectively. It can be seen from the data that under S3 condition, the first row of array of baffles attenuated the velocity of rock avalanches most, but under S2 condition, the second and third rows showed better effects on attenuating the velocity of the rock avalanches, while the velocity attenuation effect by each row of array of baffles on the rock avalanches was not much different.

Table 7 Velocity changes under different numbers of array of baffles

Condition	First row		Second row		Third row	
	V_{max} (m/s)	\bar{V} (m/s)	V_{max} (m/s)	\bar{V} (m/s)	V_{max} (m/s)	\bar{V} (m/s)
S1	5.02	3.2	2.81	2.2	2.48	1.9
S2	3.34	3.31	2.78	2.0	2.55	1.8
S3	3.47	3.1	2.96	2.3	2.51	2.0

It can be seen from Fig. 16 that as the number of baffles in each row increased, the flow distance of the rock avalanches could be increased to consume the kinetic energy of the rock avalanches. As the number of baffles increased, the drainage path inside the array of baffles increased, and the volume of the rock avalanches that could be accommodated had increased, which reduced the degree of blockage of the rock avalanches, and was more conducive to the drainage and energy consumption of the rock

avalanches. In summary, the array of baffles protection structure has a better blocking effect and drainage effect on rock avalanches under S3 working condition.

Therefore, from the numerical simulation results by the LBM, the array of baffles protection structure with the layout parameters $Sc=2.5$, $Sr=3.5$, $R_{n1}=7$, $R_{n2}=8$, $R_{n3}=9$ had better drainage and energy consumption effects.

6 Discussion

In this physical model test, the optimal layout parameter with the best blocking effect was the three-row array of baffles, with $Sc=2.5$, $Sr=4.5$. The optimized layout parameters with the best energy consumption effect of the numerical simulation results were $Sc=2.5$, $Sr=3.5$, $R_{n1}=7$, $R_{n2}=8$, $R_{n3}=9$. Regarding the optimization of the column spacing of the array of baffles, the results of physical model test and numerical simulation were similar. Under the condition of $Sc=2.5$, the deposition area of rock avalanches was the smallest, which was at least 1.7% smaller than that of other column spacing conditions, and from the particle velocity attenuation rate and velocity flow field diagram, the utilization rate and overall energy consumption of the array of baffles were the best. Regarding the optimization of the row spacing of the array of baffles, from the numerical simulation results, the utilization rate of the array of baffles and the blocking effect of the rock avalanches were the best under $Sr=3.5$; from the results of the physical model test, the deposition area of the rock avalanches was the smallest under $Sr=4.5$, which was smaller at least 6.6% than the deposition area under other row spacing conditions, and the blocking and suppression effects of rock avalanches were better. The reason for the certain gap between the two methods was that in the physical model test, the rock avalanches was all impacted from the source area to the baffle protection structure at one time, while in the numerical simulation, the rock avalanches were from the source area, and continuously impacting the array of baffles protection structure. Therefore, it caused the difference in the kinetic energy loss of the rock avalanches in the motion process, further leading to the difference in the optimization results of the row spacing Sr between the physical model test and the numerical simulation. Compared with the actual rock

avalanches, the physical model test results were closer. Regarding the number of baffles and the optimization of the number of baffles, in the physical model test, the deposition area of three rows of array of baffles was reduced by 5.3% and 4.5%, respectively compared with the deposition area of one and two rows of array of baffles. As the number of baffles increased, the width of the deposition increased and the impact distance decreased, which could effectively suppress the overall diffusion area of the rock avalanches and improve the blocking effect. Numerical simulation was used to compare the number of different baffles in the three rows of baffles. The baffle protection structure under the conditions of $R_{n1}=7$, $R_{n2}=8$, and $R_{n3}=9$ had better blocking and drainage effects on rock avalanches. The results of physical model test and numerical simulation confirmed each other, and the optimal layout parameters of the array of baffles were $Sc=2.5$, $Sr=4.5$, $R_{n1}=7$, $R_{n2}=8$, $R_{n3}=9$.

7 Conclusion

Through physical model tests, this paper analyzed in detail the influences of column spacing, row spacing, and a number of baffles on the blocking effect of the array of baffles and obtained the optimal layout parameters of the array of baffles. Using the numerical simulation based on LBM, a numerical simulation model of rock avalanches-array of baffles-hazard bearing body was built. The impact of rock avalanches on the array of baffles was numerically analyzed. Two methods were used to mutually verify the best blocking and energy consumption effects of the array of baffles protection structures against rock avalanches. The main conclusions of this research are summarized as follows:

(1) Through physical model tests, comparison was made in terms of the deposition area of rock avalanches, the siltation depth and the blocking effect. The results showed that the deposition area of the rock avalanches of three rows of baffles was reduced by 5.3% and 4.5% compared with that of one and two rows of baffles, respectively. Under the condition of $Sc=2.5$, the deposition area of the rock avalanches was the smallest, at least 1.7% smaller than that under the conditions of other column spacings. Under the condition of $Sr=4.5$, the deposition area of the rock avalanches was the smallest, at least 6.6% smaller

than that under other row spacings.

(2) Through the numerical simulation based on LBM, the velocity attenuation rate of the rock avalanches and the velocity flow field were compared. The results showed that when the array of baffles density was too large, a large amount of rock avalanches would flow from both sides of the array of baffles. As a result, the flow velocity of the rock avalanches had not been effectively alleviated; when the density of the array of baffles was small, a large number of particles passed through the array of baffles due to the too large baffle distance, posing a threat to the protection area behind. Therefore, a moderate increase in the density of the array of baffles could achieve the optimal effect of reducing the kinetic energy of rock avalanches. The optimal parameters of the numerical simulation were $Sc=2.5$, $Sr=3.5$, $R_{n1}=7$, $R_{n2}=8$, $R_{n3}=9$.

(3) By comparing the optimized layout results of the physical model test and numerical simulation, adjusting the column spacing and the number of baffles had similar influences on the energy consumption effect of rock avalanches. In terms of row spacing Sc , there was a certain difference between the results of the physical model test and numerical simulation. The difference was that the source of the numerical simulation was continuous. During the flow of the rock avalanches, it would provide a continuous kinetic energy to the rock avalanches, and the physical model test was closer to natural conditions. Therefore, in the optimization parameters of the row spacing, the physical model test results were adopted.

(4) Through physical model test and numerical simulation, the optimal layout parameters of the array of baffles with the best blocking effect were three rows of array of baffles, with $R_{n1}=7$, $R_{n2}=8$, $R_{n3}=9$, $Sc=2.5$, $Sr=4.5$. By restoring the similarity ratio with the actual project, if the velocity was close to 24.5 m/s and the flow depth was about 1.5 m, the layout parameters could be the three-row array of baffles protection structure with $Sc^*=Sc \times R \times r/h=0.85$ m, $Sr^*=Sr \times R \times r/h=1.51$ m, which played the role of optimizing the array of baffles' drainage and energy consumption effects.

In this study, a Laboratory experiment study was shown to be suitable for modeling actual rock avalanches and their interactions with array of baffles. After the LBM verification of a laboratory experiment, we performed a numerical analysis of the interaction

of rock avalanches on baffles. Many numerical experiments were conducted with particular emphasis on the influences of baffles configuration. The simulation results show that the baffles configuration have great effects on the avalanches energy consumption. Furthermore, increase the density of baffles is not necessarily better. The LBM approach

was concluded to be useful for providing qualitative information about the influences between baffles and avalanches. LBM experiments can be used to replace laboratory experiments to some extent. Further LBM-DEM studies are required before applications to practical engineering.

Acknowledgements

This research was funded by the National Natural Science Foundation of China (Grant No. 41877266, No. 41521002), the Science Foundation for Distinguished Young Scholars of Sichuan Province (Grant No.2020JDJQ0044), Scientific Research

Foundation of Graduate School of Southeast University (Grant No. YBJJ 1844), Postgraduate Research & Practice Innovation Program of Jiangsu Province (Grant No. KYCX17_0130), CAS Original Innovation Program (Grant No. ZDBS-LY-DQC039).

Reference

- Abele G (1997) Rockslide movement supported by the mobilization of groundwater-saturated valley floor sediments. *Z Geomorphol* 41(1): 1-20.
<https://doi.org/10.1127/zfg/41/1997/1>
- Ansumali S, Karlin IV, Öttinger HC (2003) Minimal entropic kinetic models for hydrodynamics. *Europhys Lett* 63(6): 798.
<https://doi.org/10.1016/j.physa.2015.10.029>
- Bettaibi S, Kuznik F, Sediki E (2016) Hybrid LBM-MRT model coupled with finite difference method for double-diffusive mixed convection in rectangular enclosure with insulated moving lid. *Physica A* 444: 311-326.
<https://doi.org/10.1016/j.physa.2015.10.029>
- Bi YZ, He SM, Li XP, et al. (2016) Geo-engineered buffer capacity of two-layered absorbing system under the impact of rock avalanches based on Discrete Element Method. *J Mt Sci* 13(5): 917-929.
<https://doi.org/10.1007/s11629-014-3354-0>
- Bi YZ, He SM, Li XP, et al. (2016b) Effects of segregation in binary granular mixture avalanches down inclined chutes impinging on defending structures. *Environ Earth Sci* 75(3): 263-264.
<https://doi.org/10.1007/s12665-015-5076-1>
- Bi YZ, He SM, Wang DP, et al. (2017) Discrete-element investigation of rock avalanches impact on the bridge pier. *Chin J Geol Hazard Control* 28(4): 16-21 (In Chinese).
<https://doi.org/10.16031/j.cnki.issn.1003-8035.2017.04.03>
- Bi YZ, Du YJ, He S M, et al. (2018) Numerical analysis of effect of baffle configuration on impact force exerted from rock avalanches. *Landslides* 15(5): 1029-1043.
<https://doi.org/10.1007/s10346-018-0979-z>
- Bi YZ, He SM, Du YJ, et al. (2019a.) Effects of the configuration of a baffle-avalanche wall system on rock avalanches in Tibet Zhangmu: discrete element analysis. *B Eng Geol Environ* 78(4): 2267-2282.
<https://doi.org/10.1007/s10064-018-1284-8>
- Bi Y Z, He S M, Du Y J, et al. (2019b) Numerical investigation of effects of “baffles-deceleration strip” hybrid system on rock avalanches. *J Mt Sci* 16(2): 414-427.
<https://doi.org/10.1007/s11629-018-4908-3>
- Bi Y Z, Sun X P, Zhao H Z, et al. (2021) Comparison Regarding the Effects of Different Baffle Systems as Impacted by Rock Avalanches. *Int J Civ Eng* 19(2): 127-144.
<https://doi.org/10.1007/s40999-020-00557-w>
- Choi CE, Ng CWW, Song D, et al. (2014) Flume investigation of landslide debris-resisting baffles. *Can Geotech J* 51(5):540-553.
<https://doi.org/10.1139/cgj-2013-0115>
- Choi CE, Cui Y, Liu LHD, et al. (2017) Impact mechanisms of granular flow against curved barriers. *Geotech Lett* 7(4): 330-338.
<https://doi.org/10.1680/jgele.17.00068>
- Fei JB, Jie YX, Sun XH, et al. (2020a) Experimental investigation on granular flow past baffle piles and numerical simulation using a μ (I)-rheology-based approach. *Powder Technol* 359: 36-46.
<https://doi.org/10.1016/j.powtec.2019.09.069>
- Fei JB, Jie YX, Hong CY, et al. (2020b) Modelling of avalanche-obstacle interaction using the depth-averaged continuum approach. *Granul Matter* 22(2): 1-15.
<https://doi.org/10.1007/s10035-020-0995-2>
- Hauksson S, Pagliardi M, Barbolini M, et al. (2007) Laboratory measurements of impact forces of supercritical granular flow against mast-like obstacles. *Cold Reg Sci Technol* 49(1): 54-63.
<https://doi.org/10.1016/j.coldregions.2007.01.007>
- Huang Y, Zhang B, Zhu C (2021) Computational assessment of baffle performance against rapid granular flows. *Landslides* 18(1): 485-501.
<https://doi.org/10.1007/s10346-020-01511-6>
- He X, Luo LS (1997) Lattice Boltzmann model for the incompressible Navier-Stokes equation. *J Stat Phys*:88(3), 927-944.
<https://doi.org/10.1023/B:JOSS.0000015179.12689.e4>
- Huang RQ, Li WL (2009) Development and distribution of geohazards triggered by the 5.12 Wenchuan Earthquake in China. *Sci China Ser E* 52(4): 810-819.
<https://doi.org/10.1007/s11431-009-0117-1>
- Huber C, Chopard B, Manga M (2010) A lattice Boltzmann model for coupled diffusion. *J Comput Phys* 229:7956-7976.
<https://doi.org/10.1016/j.jcp.2010.07.002>
- Hungr O, Evans S G, Hutchinson I N (2001) A review of the classification of landslides of the flow type. *Environ Eng Geosci* 7: 221-238.
<https://doi.org/10.2113/gseegeosci.7.3.221>
- Hungr O, Evans S G (2004) Entrainment of debris in rock avalanches: an analysis of a long run-out mechanism. *Geol*

- Soc Am Bull 116(9-10): 1240-1252.
<https://doi.org/10.1130/B25362.1>
- Jiang YJ, Towhata I (2013) Experimental study of dry granular flow and impact behavior against a rigid retaining wall. *Rock Mech Rock Eng* 46(4): 713-729.
<https://doi.org/10.1007/s00603-012-0293-3>
- Lallemand P, Luo L S (2000) Theory of the lattice Boltzmann method: dispersion, dissipation, isotropy, galilean invariance, and stability. *Phys Rev E* 61(6): 6546.
<https://doi.org/10.1103/PhysRevE.61.6546>
- Li X, Tang X, Zhao S, et al. (2020) MPM evaluation of the dynamic runout process of the giant Daguangbao landslide. *Landslides* 1-10.
<https://doi.org/10.1007/s10346-020-01569-2>
- Luo L S, Liao W, Chen X, et al. (2011) Numerics of the lattice Boltzmann method: Effects of collision models on the lattice Boltzmann simulations. *Physical Review E* 83(5): 056710.
<https://doi.org/10.1103/PhysRevE.83.056710>
- Manzella I, Labiouse V (2009) Flow experiments with gravel and blocks at small scale to investigate parameters and mechanisms involved in rock avalanches. *Eng Geol* 109(1-2): 146-158.
<https://doi.org/10.1016/j.enggeo.2008.11.006>
- Moin P, Mahesh K (1998) Direct numerical simulation: a tool in turbulence research. *Annu Rev Fluid Mech* 30(1): 539-578.
<https://doi.org/10.1146/annurev.fluid.30.1.539>
- Ng CWW, Choi CE, Kwan JSH, et al. (2014) Effects of baffle transverse blockage on landslide debris impedance. *Procedia Earth Planet Sci* 9: 3-13.
<https://doi.org/10.1016/j.proeps.2014.06.012>
- Ng CWW, Choi CE, Song D, et al. (2015) Physical modeling of baffles influence on landslide debris mobility. *Landslides* 12(1): 1-18.
<https://doi.org/10.1007/s10346-014-0476-y>
- Qi X, Yu B, Ren J (2016) Experimental study on the formation of debris flow from landslide clastic deposition. *Int J Geores Environ* 2(4): 214-226.
<https://doi.org/10.15273/ijge.2016.04.020>
- Salciarini D, Tamagnini C, Conversini P (2010) Discrete element modeling of debris-avalanche impact on earthfill barriers. *Phys Chem Earth* 35(3-5): 172-181.
<https://doi.org/10.1016/j.pce.2009.05.002>
- Succi S, Karlin IV, Chen H (2002) Colloquium: Role of the H theorem in lattice Boltzmann hydrodynamic simulations. *Rev Mod Phys* 74(4): 1203.
<https://doi.org/10.1103/RevModPhys.74.1203>
- Wen BP, Wang SJ, Wang EZ, et al. (2004) Characteristics of rapid giant landslides in China. *Landslides* 4(1): 247-261.
<https://doi.org/10.1007/s10346-004-0022-4>
- Wang D, Li Q, Bi Y, et al. (2020) Effects of new baffles system under the impact of rock avalanches. *Eng Geol* 264: 105261.
<https://doi.org/10.1016/j.enggeo.2019.105261>
- Wang F, Chen X, Chen J, et al. (2017) Experimental study on a debris-flow drainage channel with different types of energy dissipation baffles. *Eng Geol* 220: 43-51.
<https://doi.org/10.1016/j.enggeo.2017.01.014>
- Yang X, Shi B, Chai Z (2014) Coupled lattice Boltzmann method for generalized Keller-Segel chemotaxis model. *Comput Math Appl* 68:1653-1670.
<https://doi.org/10.1016/j.camwa.2014.10.023>
- Zanuttigh B, Di Paolo A (2006) Experimental analysis of the segregation of dry avalanches and implications for debris flows. *J Hydraul Res* 44(6):796-806.
<https://doi.org/10.1080/00221686.2006.9521730>
- Zhao T, Crosta GB, Urti S, et al. (2017) Investigation of rock fragmentation during rockfalls and rock avalanches via 3 - D discrete element analyses. *J Geophys Res: Earth Surface* 122(3): 678-695.
<https://doi.org/10.1002/2016JF004060>
- Zhou L, Qu ZG, Ding T, et al. (2016) Lattice Boltzmann simulation of the gas-solid adsorption process in reconstructed random porous media. *Phys Rev E* 2016: 93(4): 043101.
<https://doi.org/10.1103/PhysRevE.93.043101>
- Zou Q, He X (1997) On pressure and velocity boundary conditions for the lattice Boltzmann BGK model. *Phys Fluids* 9(6): 1591-1598.
<https://doi.org/10.1063/1.869307>